Determination of thermodynamic stability of lanthanum chloride hydrates (LaCl₃·xH₂O) by dynamic transpiration method

Deepak Kumar Sahoo [a], R. Mishra [b,*], H. Singh [a], N. Krishnamurthy [c]

[a] Rare Earths Development Section, Bhabha Atomic Research Centre, Trombay, Mumbai 400 085, India
[b] Chemistry Division, Bhabha Atomic Research Centre, Trombay, Mumbai 400 085, India
[c] Fusion Reactor Materials Section, Bhabha Atomic Research Centre, Trombay, Mumbai 400 085, India

A B S T R A C T

The decomposition pattern of $LaCl_3 \cdot 7H_2O(s)$ was studied by thermogravimetric technique. Thermal decomposition of $LaCl_3 \cdot 7H_2O(s)$ proceeded through the formation of $LaCl_3 \cdot 3H_2O(s)$, $LaCl_3 \cdot H_2O(s)$ and $LaCl_3(s)$ in the temperature range 313 to 413 K. Thermodynamic stability of the $LaCl_3 \cdot 7H_2O(s)$ and its intermediate products were determined by measuring the vapor pressure of water over the compounds employing dynamic transpiration technique. Two independent sets of experiments were carried out to measure the vapor pressure of each step. The average vapor pressure of $H_2O(g)$ over $LaCl_3 \cdot 7H_2O(s)$, $LaCl_3 \cdot 3H_2O(s)$ and $LaCl_3 \cdot H_2O(s)$ could be expressed by the relations: $\ln p_{H_2O}/atm$ $(\pm 0.02) = -7422$ $(\pm 211)/T + 17.5$ (± 0.6) $(327 \leqslant T/K \leqslant 334)$, $\ln p_{H_2O}/atm$ $(\pm 0.02) = -8287(\pm 566)/T + 17.5$ (± 1.5) $(365 \leqslant T/K \leqslant 369)$ and $\ln p_{H_2O}/atm$ $(\pm 0.01) = -8566(\pm 346)/T + 16.4(\pm 1)$ $(391 < T/K < 396)$. The standard molar Gibbs energy of formation of $LaCl_3 \cdot 7H_2O(s)$, $LaCl_3 \cdot 3H_2O(s)$ and $LaCl_3 \cdot H_2O(s)$ derived from the vapor pressure data are found to be: $\Delta_f G°(LaCl_3 \cdot 7H_2O,s) = -3226$ $(\pm 13) + 1.6(\pm 0.1)T$ $(327 \leqslant T/K < 334)$, $\Delta_f G°(LaCl_3 \cdot 3H_2O,s) = -2006(\pm 11) + 0.8(\pm 0.1)T$ $(365 \leqslant T/K \leqslant 369)$ and $\Delta_f G°(LaCl_3 \cdot H_2O,s) = -1383(\pm 10) + 0.4(\pm 0.01) \cdot T$ $(391 < T/K < 396)$, kJ mol⁻¹, respectively.

© 2013 Elsevier B.V. All rights reserved.

1. Introduction

Lanthanum and its alloys have attracted a lot of attention in recent years for their wide applications in the fields of electronics, magnetic and hydrogen storage materials [1–3]. The element is effective in improving the corrosion resistant properties of stainless steel and magnesium, aluminum bearing alloys [4,5]. One of the most important aspects in the preparation of lanthanum metal is the quality of precursor used in the production process. Anhydrous lanthanum chloride is widely used as the precursor for producing lanthanum metal in chemical and electrolytic reduction processes [6–8]. Lanthanum chloride is highly hygroscopic in nature and absorbs moisture when exposed to atmosphere even for short duration. The compound can absorb more than 34 wt% crystallized water and adsorbed moisture. Anhydrous lanthanum chloride is prepared by heating hydrated lanthanum chloride for several hours in vacuum or under flowing inert gas [9,10]. The main difficulty in obtaining anhydrous lanthanum chloride in pure form is the formation of small amount of lanthanum oxychloride $LaOCl(s)$ during dehydration process through the reaction $LaCl_3 \cdot nH_2O(s) \rightarrow LaOCl(s) + 2HCl(g) + (n-1)$ $H_2O(g)$. Presence of lanthanum oxychloride impairs the reduction process and thereby

affects both yield and product purity. Therefore, it is necessary to find out an effective way to remove moisture from the starting material. Knowledge of thermodynamic stability of the lanthanum chloride hydrates and the mechanism of the dehydration processes is of great interest for the production of anhydrous chloride.

The mechanism of dehydration of hydrated lanthanum chloride has been studied by many researchers [11–16]. Powel and Burkholder [13] reported the existence of intermediates such as $LaCl_3 \cdot 3H_2O(s)$ and $LaCl_3 \cdot H_2O(s)$. The decomposition pattern of $LaCl_3 \cdot 7H_2O$ due to loss of water reported by Ashcroft and Mortimer [14] was found to $LaCl_3 \cdot 7H_2O(s) \rightarrow LaCl_3 \cdot 3H_2O(s) \rightarrow LaCl_3 \cdot 2H_2O \rightarrow LaCl_3 \cdot H_2O(s) \rightarrow LaCl_3(s)$. Hong and Sundstrom [15] have shown the dehydration scheme as $LaCl_3 \cdot 7H_2O(s) \rightarrow LaCl_3 \cdot 3H_2O(s) \rightarrow LaCl_3 \cdot H_2O(s) \rightarrow LaCl_3(s)$. Ren et.al. [16,17] have described the dehydration scheme of $LaCl_3 \cdot 7H_2O(s)$ with the following steps: $LaCl_3 \cdot 7H_2O(s) \rightarrow LaCl_3 \cdot 6H_2O(s) \rightarrow LaCl_3 \cdot 3H_2O(s) \rightarrow LaCl_3 \cdot H_2O \rightarrow LaCl_3(s)$ and also have reported that dehydration at higher temperature lead to formation of small amount of $LaOCl(s)$.

In view of the conflicting reports on the decomposition pattern of $LaCl_3 \cdot 7H_2O$, the sequence of decomposition was reinvestigated in the present study by thermal and high temperature X-ray techniques.

In the present work, the equilibrium vapor pressure of water over various hydrates was measured employing dynamic transpiration technique. The standard molar Gibbs energy of formation of

---

* Corresponding author. Tel.: +91 22 2559 2460.
E-mail address: mishrar@barc.gov.in (R. Mishra).

lanthanum chloride hydrates have been derived using the measured equilibrium vapor pressure data. The derived thermodynamic properties have been compared with the existing literature [18–27]. This information may be useful in fixing the conditions for dehydration of LaCl$_3$·7H$_2$O(s) to form LaCl$_3$(s) free of oxychloride.

2. Experimental

LaCl$_3$·7H$_2$O(s) (99.99% purity) used for the vapor pressure measurement experiments was supplied by Indian Rare Earth Limited (IREL). The sample was characterized by thermal and X-ray diffraction (XRD) techniques. Thermogravimetry, differential thermal analysis, evolved gas analysis studies were carried out in a SETARAM (Setsys Evolution, France) TG–DTA–EGA instrument at heating rates of 0.5, 2, 5 and 10 K/min in flowing argon atmosphere. Room temperature and high temperature XRD studies were carried out employing a Phillips High Temperature X-ray diffractometer (HT-XRD) (Panalytical X-pert-pro) using Cu Kα radiation. HT-XRD patterns were recorded at 30, 75, 105, 140 and 180 °C in the 2θ range 10–80° in static air atmosphere. The sample spread over platinum metal substrate using collodion solution was heated at a heating rate 5 K/min and held constant at the pre-determined temperature with ±0.5 accuracy during the measurement.

2.1. Vapor pressure measurement

The thermodynamic stability of the LaCl$_3$·7H$_2$O(s) and its decomposed products such as LaCl$_3$·6H$_2$O(s), LaCl$_3$·3H$_2$O(s) and LaCl$_3$·H$_2$O(s) were determined by measuring vapor pressure of H$_2$O(g) over the compounds by a novel dynamic thermogravimetric transpiration instrument using a micro-thermo balance (SETARAM, Model B24) described elsewhere [28]. In the present experiment the vapor pressure of water (p_{H_2O}) was determined from the total mass loss (Δm) recorded at constant temperature (T) for known time interval (t) and carrier gas flow rate (v), following the equation P$_{H_2O}$ = $\Delta m/t \times 1/M_{H_2O} \times RT/v$, where M_{H_2O} is the molecular weight of water, T is the room temperature and R is the universal gas constant. Fig. 1 gives the sketch diagram of the micro-thermo balance assembly used in the present study. A Pt, Pt-10%Rh thermocouple used for measuring the sample temperature was located about 1 mm away from the sample well within the isothermal zone of the reaction tube. The equilibrium condition for the measurement of vapor pressure was established by monitoring the mass loss of the sample per unit volume of the carrier gas (argon) swept over it as a function of flow rate at the mean temperatures of mass loss corresponding to each vaporization step. The region where the apparent vapor pressure of water is independent of flow rate of the carrier gas was determined to ascertain the saturation of the carrier gas by the vapor. The measurement of vapor pressure at different temperatures was carried out using the constant flow rate of the carrier gas in the plateau region.

In the present case due to narrow temperature range stability and highly hygroscopic nature of the intermediate compounds, it was difficult to isolate the decomposed products and to establish the respective coexisting phase fields separately. Therefore, we have tried to obtain the sample with desired composition in the two phase region of the given vaporization reaction in situ. This was done by monitoring the total mass loss from the sample carried out in the transpiration apparatus using direct program mass loss technique. During vapor pressure measurement the mass loss was confined to 10 to 50% of the total expected mass loss for the corresponding steps. We presumed here that during the first 10 wt% loss process, the contributions due to the mass loss from the previous step gets over and by confining the measurements within 50 wt% loss, the kinetic hindrances of decomposition at higher percentage of mass loss is avoided. Further, it was assumed that there is no mutual solubility of among the co-existing phases during the vaporization reaction and the activity of the each of the solid phase is unity.

The temperature coefficient of vapor pressure was determined by dynamic transpiration technique measured at a constant flow rate (2.4 l/h), at a heating rate of 0.5 K/min recorded in the temperature range 326–398 K. The sample was spread on a double stranded platinum crucible to increase the surface area. For calculation of vapor pressure, the mass loss was considered for the time interval of 60–80 s at a given mean temperature. Since the heating rate was maintained at a rate 0.5 K/min, in the time interval of 60–80 s the maximum variation in the temperature is expected to be 0.5–0.8 K which is well within the experimental uncertainty of temperature measurements. Therefore, it can be assumed that the mass loss process is nearly isothermal for a given measurement. The plots of the observed mass loss with respect to time in isothermal runs at given flow rate (2.4 l/h) of the carrier gas were used to calculate the vapor pressure. Measurements were carried out in the temperature range of 327–334 K, 365–369 K and 391–396 K, for the two-phase mixtures LaCl$_3$·7H$_2$O(s) + LaCl$_3$·3H$_2$O(s) and LaCl$_3$·3H$_2$O(s) + LaCl$_3$·H$_2$O(s) and LaCl$_3$·H$_2$O(s) + LaCl$_3$(s), respectively.

3. Results and discussion

Fig. 2 gives the TG plot of LaCl$_3$·7H$_2$O(s) recorded at the heating rates of 0.5, 2, 5 and 10 K/min under 2 l/h flowing argon

atmosphere. The figure indicates that the compound undergo mass losses in three successive steps corresponding to the loss of 4, 2 and 1 number of water molecules. From Fig. 2, it could also be observed that the decomposition temperature for each mass loss step is heating rate (β) dependent and progressively decrease with decrease in β. Fig. 3 gives the plot decomposition temperature versus heating rate for step-1, step-2 and step-3 of LaCl$_3$·7H$_2$O decomposition. The extrapolated decomposition temperatures to zero heating rate for step-1, step-2 and step-3 are found to be 41, 86 and 120 °C respectively and the corresponding temperature ranges for mass loss steps are found to be 41–75 °C, 86–105 °C and 120–140 °C, respectively. DTA plot of the sample showed three endothermic peaks with initiation temperatures 41, 85 and 120 °C, which correspond to the endothermic effects caused by the loss of 4, 2 and 1 water molecules in mass loss step-1, step-2 and step-3 respectively. The decomposition temperatures obtained from this work are found to be significantly lower compared to the earlier reported values [16,17]. This could be due to higher heating rate leading to non-equilibrium decomposition of lanthanum hydrate. In order to ascertain the decomposition temperature, high temperature X-ray diffraction patterns were recorded at the end each decomposition step. Fig. 4a gives the HTXRD patterns of LaCl$_3$·7H$_2$O(s) at room temperature and its decomposed daughter products recorded at 75 and 105 °C whereas Fig. 4b gives XRD patterns at 140 and 180 °C, which corresponds to LaCl$_3$. The XRD patterns at room temperature and 75 °C are found to match well with the reported pattern of LaCl$_3$·7H$_2$O(s) (JCPDF # 03–0069), LaCl$_3$·3H$_2$O(s) (JCPDF # 82–1200). However, the XRD plot for the compound LaCl$_3$·H$_2$O recorded at 105 does not have any reported pattern for comparison. The XRD pattern recorded at 140 and 180 °C matched well with reported pattern of LaCl$_3$(s) (JCPDF #73–2063) with some peaks due to LaOCl. The small amount of LaOCl(s) present in the sample could be due to the reaction of the water vapor with freshly produced LaCl$_3$(s) in static air condition. The formation of LaOCl(s) may not be possible when the water vapor is effectively flushed out in the present case. Further, Fig. 4 indicates that the room temperature pattern has sharp and well defined XRD peaks and the peak intensity and sharpness decreases as sample temperature of the sample increases. This is due to progressive loss of water molecules crumbling of the crystal structure and formation new crystal lattice with smaller crystallite size. No line due parent compound could be seen all these XRD patterns, which is in confirmation with our TG results. Evolved gas analysis (Fig. 5) of the sample indicates the loss of only water molecule over the entire range of mass loss steps. No mass peak for the mass numbers 36 and 38 due to HCl molecules produced by the hydrolysis of the LaCl$_3$(s) with the evolved water vapor could be observed. The onset temperatures for different mass loss steps was further verified by recording TG–DSC (Mettler Toledo, TG–DSC-1) run at heating rate of 0.5 K/min under 2 l/h flowing argon in a commercial instrument.

From Fig. 2(a) it could be observed that the sample decomposes in three successive steps in the temperature ranges 41–75 °C, 86–105 °C and 120–140 °C, respectively with 19.5%, 9.5% and 4.8% mass loss respectively. The 19.5% mass loss in the first step is attributed to loss of four water molecules. Similarly, 9.7% and 4.8% mass loss observed in the second and third steps correspond to the loss of two and one water molecules, respectively. Table 1 gives the comparison of measured and calculated mass loss for different vaporization steps. Based on the above observations the decomposition mechanism of the LaCl$_3$·7H$_2$O can be described as

$$LaCl_3 \cdot 7H_2O(s) \rightarrow LaCl_3 \cdot 3H_2O(s)$$
$$+ 4H_2O(g) \quad (314/T/K/348) \quad (1)$$
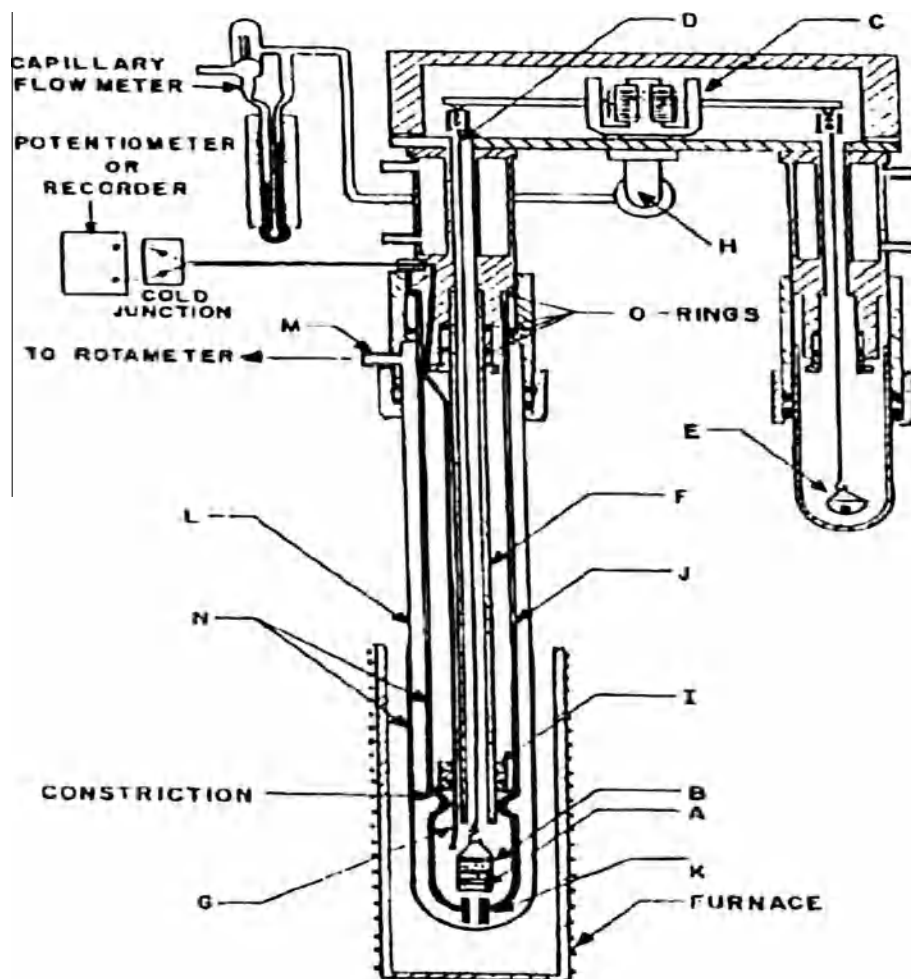
Fig. 1. Sketch diagram of micro thermo-balance assembly used for dynamic transpiration vapor measurements, where **A**. Sample, **B**. Tired sample holder, **C**. Electronic recording-type microbalance, **D**. Hangdown wire (0.2 mm in diameter), **E**. Silica pan for weight taring), **F**. 4 mm internal diameter (ID) silica tube, **G**. Thermocouple, **H**. Rear port in the balance housing, **I**. Baffles made of (i) Pt-20%Rh plate and (ii) alumina discs, **J**. 14 mm ID silica tube, **K**. capillary (1.5 mm diameter hole), **L**. 28 mm ID silica tube, **M**. 8 mm diameter hole, **N**. Layers of platinum coating. Details of the assembly are explained in Ref. [28].
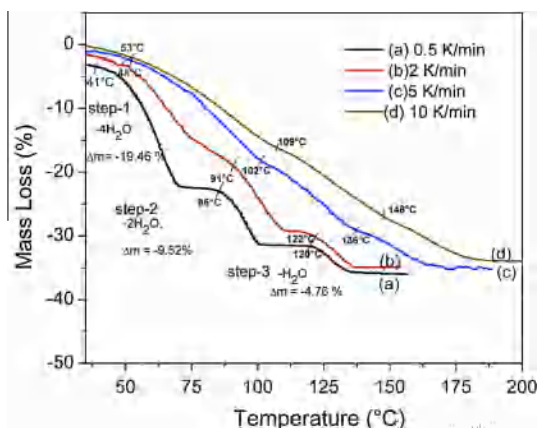
Fig. 2. TG plot of LaCl$_3$·7H$_2$O recorded at the heating rate of 0.5, 2, 5 and 10 K/min under 2 l/h flowing argon atmosphere.

Fig. 3. Plot decomposition temperature versus heating rate for step-1, step-2 and step-3 of LaCl$_3$·7H$_2$O decomposition.

$$LaCl_3 \cdot 3H_2O(s) \rightarrow LaCl_3 \cdot H_2O(s) + 2H_2O(g) \quad (359/T/K/378) \quad (2)$$

$$LaCl_3 \cdot H_2O(s) \rightarrow LaCl_3(s) + H_2O(g) \quad (390/T/K/413). \quad (3)$$
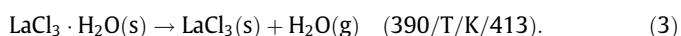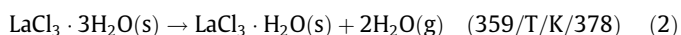
The above mechanism of decomposition of LaCl$_3$·7H$_2$O matches well with the reported data [15].
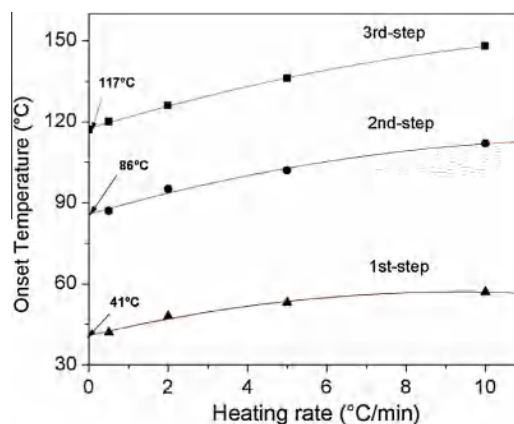
3.1. Vapor pressure analysis

Fig. 6 gives the apparent pressure versus flow rate of the carrier gas for LaCl$_3$·7H$_2$O(s) → LaCl$_3$·3H$_2$O(s) + 4H$_2$O(g) reaction measured at 330 K for Eq. (1). From the figure it can be observed that the apparent pressure of water over the sample is independent of
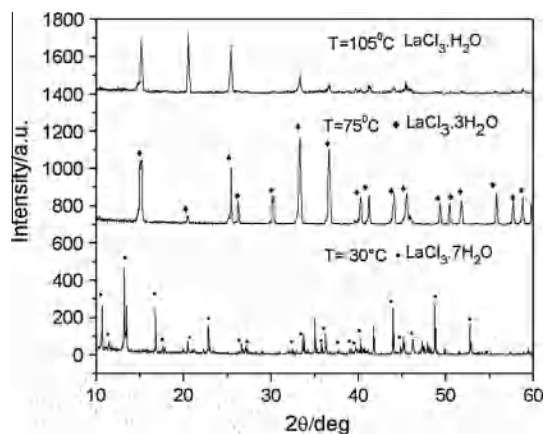
Fig. 4a. HTXRD patterns of LaCl$_3$·xH$_2$O(s) sample recorded at 30, 75 and 105 °C.
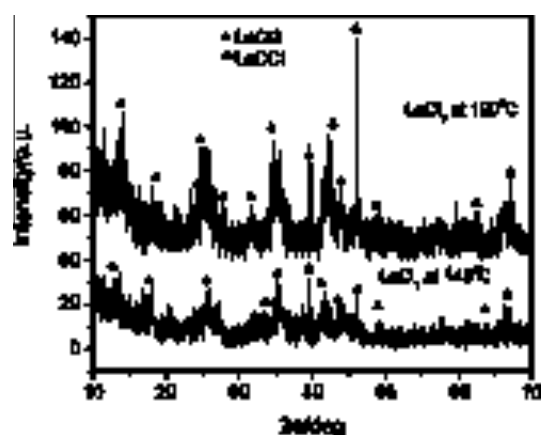
Fig. 4b. HTXRD patterns of LaCl$_3$(s) sample recorded at 140 and 180 °C.
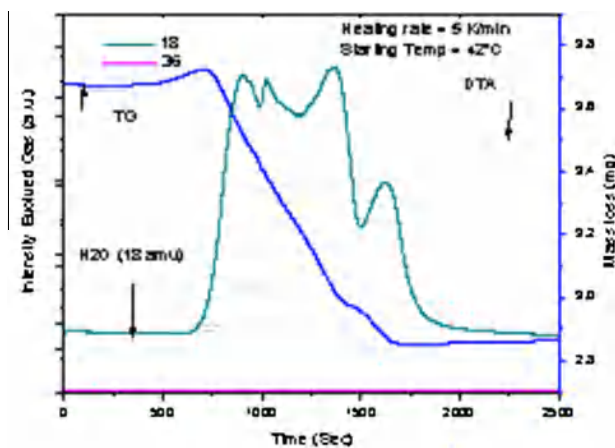
Fig. 5. TGA–EGA plot of LaCl$_3$·7H$_2$O recorded at the heating rate of, 5 K/min under 2 l/h flowing argon atmosphere.

flow rate of the carrier gas in the flow rate region, 1.9–2.7 l/h, indicating the establishment of equilibrium condition. A carrier gas flow rate of 2.4 l/h was therefore, chosen in the vapor pressure measurement experiments. Similar experiments were carried for the vaporization reactions given in Eqs. (2) and (3) under exactly similar conditions. Care was taken in all these steps to restrict the total mass loss in the range 10–50% of the expected weight loss in respective cases. It was observed that in all these steps the flow rate independent region of the apparent pressure (plateau) also falls within 1.9–2.7 l/h. Hence a constant flow rate of 2.4 l/h was chosen for the measurement of temperature coefficient of vapor pressure in all the cases. Another similar experiments was carried out at same flow rate to ascertain the reproducibility

The vapor pressure of water as function of temperature was calculated from the rate of mass loss for given volume of carrier gas passed over the sample. Table 2 gives the mass loss data for vaporization steps 1, 2 and 3, respectively for experiments 1 and 2. The plots of ln p$_{H_2O}$ versus 1/T for the above processes are given in Fig. 7(a–c). The least square fitted linear equations could be expressed as:

$$\ln p_{H_2O}/Pa(\pm 0.02) = -7422(\pm 211)/T + 17.5(\pm 0.6) \quad (327 \leqslant T/K \leqslant 334) \tag{4}$$

$$\ln p_{H_2O}/Pa(\pm 0.03) = -8287(\pm 566)/T + 17.5(\pm 1.5) \quad (365 \leqslant T/K \leqslant 369) \tag{5}$$

and

$$\ln p_{H_2O}/atm(\pm 0.01) = -8566(\pm 346)/T + 16.4(\pm 1) \quad (391 < T/K < 396). \tag{6}$$

The average standard molar enthalpies and entropies of vaporization for the respective reactions described in Eqs. (1)–(3) calculated from the slope of the plots are given in Table 3 and have been compared with the available literature.

3.2. Gibbs energy of formation

The Gibbs energy of formation ($\Delta_f G°$) of LaCl$_3$·7H$_2$O and its decomposition products such as LaCl$_3$·3H$_2$O and LaCl$_3$·H$_2$O were calculated using the measured equilibrium vapor pressures of water over the samples and the value of standard Gibbs energy of formation of LaCl$_3$ from literature [29]. Considering LaCl$_3$(s) as anchoring point, the value of $\Delta_f G°$ of the co-existing phase LaCl$_3$·H$_2$O was first derived by using the vapor Eq. (6), following the reaction LaCl$_3$·H$_2$O(s) → LaCl$_3$(s) + H$_2$O(g). The free energy change for the reaction, $\Delta G°r = -RT\ln K$, where K is the equilibrium constant for the vaporization reaction can be expressed as

$$\Delta G°r = \Delta_f G°(LaCl_3, s) + \Delta_f G°(H_2O, g) - \Delta_f G°(LaCl_3 \cdot H_2O, s).$$

Equating $\Delta G°_r = RT\ln p_{(H_2O)}/atm$ and on rearranging the above equation, the free energy of formation of LaCl$_3$·H$_2$O(s) could be expressed as

$$\Delta_f G°(LaCl_3 \cdot H_2O, s) = \Delta_f G°(LaCl_3, s) + \Delta_f G°(H_2O, g) + RT\ln p(H_2O)/atm.$$

Table 1
Measured and calculated mass loss for different vaporization reaction steps of LaCl$_3$·7H$_2$O.

Reaction steps	Temperature range (K)	Measured mass loss (%)	Vaporization reaction	Calculated mass loss (%)
1	314–348	19.5	LaCl$_3$·7H$_2$O(s) → LaCl$_3$·3H$_2$O(s) + 4H$_2$O(g)	19.2
2	359–378	9.7	LaCl$_3$·3H$_2$O(s) → LaCl$_3$·H$_2$O(s) + 2H$_2$O(g)	9.6
3	390–413	4.8	LaCl$_3$·H$_2$O(s) → LaCl$_3$(s) + H$_2$O(g)	4.8

Table 2
Mass loss data for the step-1, step-II and step-III of the vaporization reactions measured at carrier gas flow rate of 2.4 l/h.

Mass loss step	Experiments	Average temp. (T/K)	Mass loss ($\Delta m/\mu g$)	Time ($\Delta t/s$)	Apparent pressure $P(H_2O)$/atm
Step-I	Expt.1	327	220	85	0.00527
		328	255	90	0.00577
		329	231	75	0.00628
		330	283	85	0.00678
		331	354	100	0.00721
		332	303	80	0.00772
		333	318	80	0.0081
		334	416	100	0.00848
	Expt.2	327	182	70	0.0053
		328	226	80	0.00576
		329	230	75	0.00625
		331	231	65	0.00724
		332	266	70	0.00774
		333	337	85	0.00808
		334	292	70	0.0085
Step-II	Expt.1	365	180	65	0.00564
		366	166	55	0.00615
		367	244	75	0.00663
		368	172	50	0.00701
		369	264	75	0.00717
	Expt.2	365	194	70	0.00565
		366	225	75	0.00611
		367	261	80	0.00665
		368	240	70	0.00699
		369	265	75	0.0072
Step-III	Expt.1	391.5	146	71.5	0.00416
		392.5	127	58.5	0.00442
		393.5	151	65	0.00473
		394.5	192	78	0.00502
		395.5	180	71	0.00517
	Expt.2	391.5	154	75	0.00418
		392.5	151	70	0.0044
		393.5	174	75	0.00473
		394.5	171	70	0.00498
		395.5	203	80	0.00517
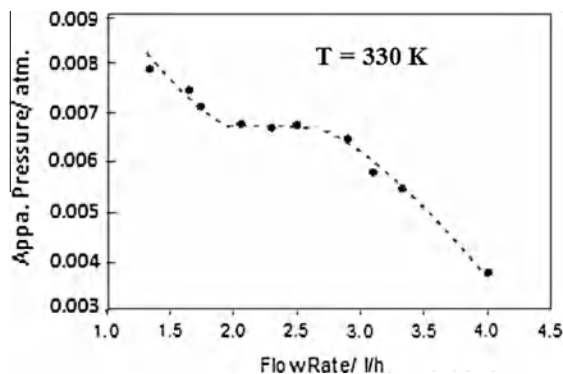
Fig. 6. The apparent pressure versus flow rate of the carrier gas for LaCl$_3$·7H$_2$O(s) LaCl$_3$·3H$_2$O(s) + 4H$_2$O(g) reaction measured at 330 K.

Putting the value of $\ln p_{(H_2O)}$ for the above vaporization reaction from Eq. (6) and values of standard Gibbs free energy of formation of LaCl$_3$(s) and H$_2$O(g) from the literature [21], the molar Gibbs free energy of formation of LaCl$_3$·H$_2$O was found to be

$$\Delta_f G^\circ (LaCl_3 \cdot H_2O, s)(\pm 0.03) \text{ kJ mol}^{-1}$$
$$= -1381(\pm 10) + 0.43(\pm 0.01) T \ (391 < T/K < 396). \quad (7)$$

The standard deviation of Gibbs free energy of formations was derived from the least square fitting of experimental data only.

The standard molar Gibbs energy of formation of LaCl$_3$·3H$_2$O(s) was similarly derived following the vaporization reaction LaCl$_3$·3H$_2$O(s) → LaCl$_3$·H$_2$O(s) + 2H$_2$O(g). The expression for free energy of the compound in terms of vapor pressure of H$_2$O could be expressed as

$$\Delta_f G^\circ (LaCl_3 \cdot 3H_2O, s) = \Delta_f G^\circ (LaCl_3 \cdot H_2O, s) + 2\Delta_f G^\circ (H_2O, g)$$
$$+ 2RT \ln p_{(H_2O)}/\text{atm}.$$

Putting the value of $\ln p_{(H_2O)}$ for the above vaporization reaction from Eq. (7), the value of standard Gibbs free energy of formation of LaCl$_3$·H$_2$O(s) derived from previous section and H$_2$O(g) from the literature [21], the molar Gibbs free energy of formation of LaCl$_3$·3H$_2$O was found to be

$$\Delta_f G^\circ (LaCl_3 \cdot 3H_2O, s)(\pm 0.03) \text{ kJ mol}^{-1}$$
$$= -2006(\pm 11) + 0.8(\pm 0.1)T(365 \leqslant T/K \leqslant 369). \quad (8)$$

Similarly the standard molar Gibbs energy of LaCl$_3$·7H$_2$O(s) was derived by considering the vaporization reaction LaCl$_3$·7H$_2$O(s) → LaCl$_3$·3H$_2$O(s) + 3H$_2$O(g) (Eq. (1)). The expression LaCl$_3$·7H$_2$O(s) in terms of vapor pressure of H$_2$O could be expressed as

$$\Delta_f G^\circ (LaCl_3 \cdot 7H_2O, s) = \Delta_f G^\circ (LaCl_3 \cdot 3H_2O, s) + 4\Delta_f G^\circ (H_2O, g)$$
$$+ 4RT \ln p(H_2O)/\text{atm}.$$

Putting the values of $\ln p(H_2O)$ from Eq. (4), standard Gibbs free energy of formation of LaCl$_3$·3H$_2$O(s) and Gibbs energy of formation H$_2$O(g) the standard Gibbs free energy of formation of LaCl$_3$·7H$_2$O(s) could be expressed as

$$\Delta_f G^\circ (LaCl3 \cdot 7H_2O, s)(\pm 0.06) \text{kJmol}^{-1}$$
$$= -3226(\pm 13) + 1.6(\pm 0.1)T(327 \leqslant T/K \leqslant 334). \quad (9)$$
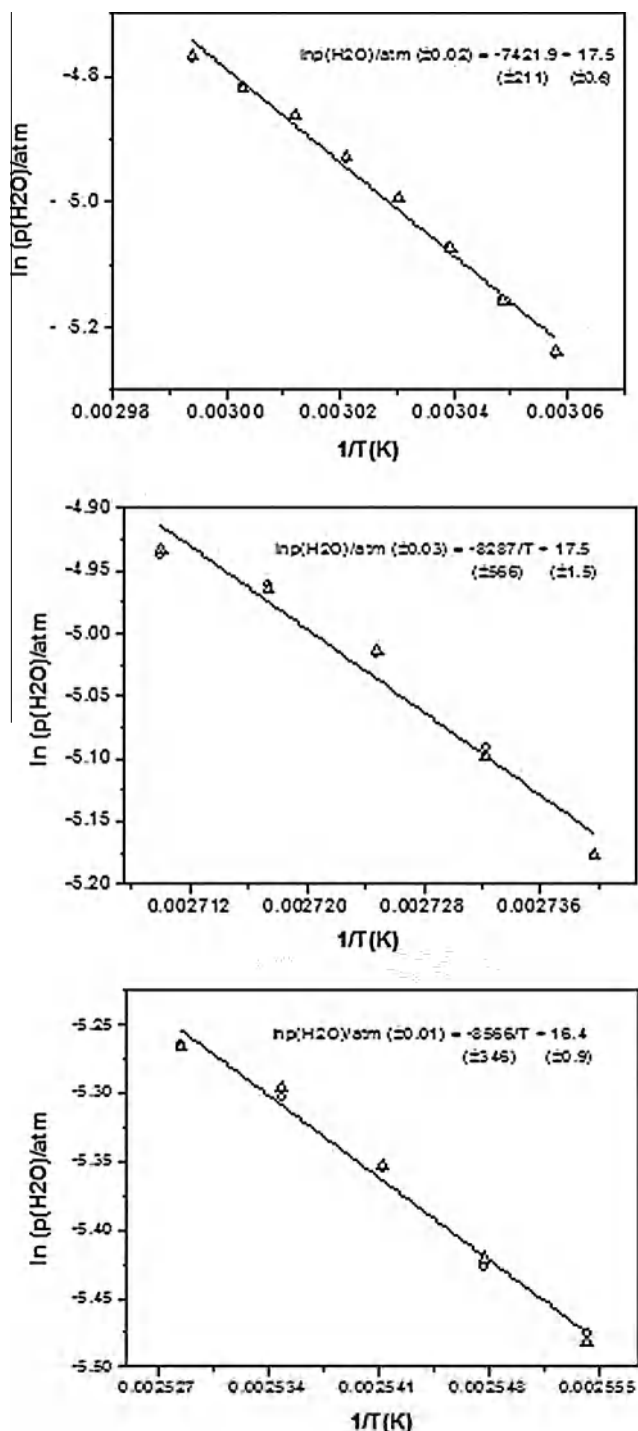
Fig. 7. Plots of lnp versus 1/T for the vaporization reaction $LaCl_3 \cdot 7H_2O(s) \rightarrow LaCl_3 \cdot 3H_2O(s) + 4H_2O(g)$ (step-I), $LaCl_3 \cdot 3H_2O(s) \rightarrow LaCl_3 \cdot H_2O(s) + 2H_2O(g)$ (step-II) and $LaCl_3 \cdot H_2O(s) \rightarrow LaCl_3(s) + H_2O(g)$ (step-III).

Table 4
Comparison of values of standard molar enthalpies of formation of $LaCl_3 \cdot 7H_2O(s)$, $LaCl_3 \cdot 3H_2O(s)$, $LaCl_3 \cdot H_2O(s)$.

Compounds	T mean (T/ K)	$\Delta_f H^0$ (kJmol^{-1}) (This work)	$\Delta_f H^0$ (kJ mol^{-1}) (literature)
$LaCl_3 \cdot 7H_2O$	329	−3226 ± 13	−3182 Ref. [19]
$LaCl_3 \cdot 3H_2O$	367	−2006 ± 11	−1985 Ref. [27]
$LaCl_3 \cdot H_2O$	393	−1381 ± 10	−1381 Ref. [18]

The standard molar enthalpy of formation of $LaCl_3 \cdot 7H_2O(s)$, $LaCl_3 \cdot 3H_2O(s)$ and $LaCl_3 \cdot H_2O(s)$ at the mean temperature of measurements i.e. 329 K, 367 K and 393 K are found to be −3226 ± 13, −2006 ± 11 and −1381 ± 10 kJ mol^{-1}, respectively. The standard molar entropies of formation at the mean temperature of measurement are found to be −1600 ± 100, −800 ± 100 and −430 ± 100 J mol^{-1} K^{-1}, respectively. The values of standard molar enthalpies of formation of $LaCl_3 \cdot 7H_2O(s)$, $LaCl_3 \cdot 6H_2O(s)$, $LaCl_3 \cdot 3H_2O(s)$, and $LaCl_3 \cdot H_2O$ have been compared with the available literature in Table 4.

In absence of heat capacity information on hydrated lanthanum chloride system, the values of standard molar enthalpy of formation hydrated lanthanum chlorides at the mean temperature of measurement are compared with the standard molar enthalpy of formation ($\Delta_f H^\circ_{298.15}$ reported in the literature. The values of standard molar enthalpy of formation of $LaCl_3 \cdot H_2O$ −1381 ± 10 kJ mol^{-1} at 329 K is found to agree well with the reported value of $\Delta_f H^\circ_{298.15}$ = −1381.4 kJ mol^{-1} [18]. Similarly the standard molar enthalpy of formation of $LaCl_3 \cdot 3H_2O$ at 367 K is found to −2006 ± 11 kJ mol^{-1} agrees well with the available data for this compound [27]. The standard molar enthalpy of formation of $LaCl_3 \cdot 7H_2O$ at the mean temperature 393 K is found to be −3226 ± 13 kJ mol^{-1} which is also comparable with the reported value of −3182 kJ mol^{-1} [23].

The calorimetrically determined enthalpy change for the reaction $LaCl_3 \cdot 7H_2O = LaCl_3(s) + 7H_2O(g)$ as reported in the literature [20–22] is 417.8 kJ mol^{-1}, where the enthalpy change for the reaction calculated from the present data is 461.8 ± 18 kJ mol^{-1}. The difference in the enthalpy of reaction as compared to the calorimetric value can be attributed to the evaporation loss of adsorbed water in the first step.

4. Summary

The decomposition pattern of $LaCl_3 \cdot 7H_2O$ was established by thermogravimetric technique. The thermodynamic stability of the $LaCl_3 \cdot 7H_2O$ and the intermediate compounds were determined. Thermodynamic stability of lanthanum chloride hydrates presented in this paper has been compared with the available literature.

Acknowledgement

Table 3
Comparison of values of standard molar enthalpies and entropies for the vaporization reaction steps 1, 2 and 3.

Reaction steps	Vaporization reaction	$\Delta H^\circ r$ (kJ mol^{-1}) (this work)	$\Delta H^\circ r$ (kJ mol^{-1}) (Literature)	$\Delta S^\circ r$ (J mol^{-1} K^{-1}) (this work)	$\Delta S^\circ r$ (J mol^{-1} K^{-1}) (Literature)
1	$LaCl_3 \cdot 7H_2O = LaCl_3 \cdot 3H_2O(s) + 4H_2O(g)$	246.8 ± 1.7	229.8 Refs. [20–22]	581.8 ± 4	569.4 Refs. [20,23–25]
2	$LaCl_3 \cdot 3H_2O(s) = LaCl_3 \cdot H_2O(s) + 2H_2O(g)$	141.4 ± 4.7	120.4 Refs. [20–22]	290.8 ± 12	284.7 Refs. [20,23–25]
3	$LaCl_3 \cdot H_2O(s) = LaCl_3(s) + H_2O(g)$	72.5 ± 2.9	72.5 Refs. [20–22]	136.3 ± 8	142.4 Refs. [20,23–25]

References

[1] W.J. Głuchowski, Z.M. Rdzawski, J. Achievements Mater. Manuf. Eng. 24 (2007) 103–106.
[2] M.Q. Huang, S. Simizu, B. Zande, V.K. Chandhok, R. Obermyer, W.E. Wallace, S.G. Sankar, IEEE Trans. 37 (2001) 2537–2539.
[3] H. Zhang, Y. Chen, S. Li, X. Fu, Y. Zhu, S. Yi, X. Xue, Y. He, Y. Chen, J. Appl. Phys. 94 (2003) 6417–6422.
[4] M. Fukumoto, R. Yamashita, M. Hara, Oxid. Met. 62 (2004) 309–322.
[5] R.Z. Wu, Y.S. Deng, M.L. Zhang, J. Mater. Sci. 44 (2009) 4132–4139.
[6] R. Sharma, JOM 39 (1987) 33–37.
[7] T. Yamamura, M. Mehmood, H. Maekawa, Y. Sato, Chem. Sust. Dev. 12 (2004) 105–111.
[8] L. Feng, C. Guo, D. Tang, J. Alloys Comp. 234 (1996) 183–186.
[9] C.K. Gupta, N. Krishnamurthy, Int. Mater. Rev. 37 (1992) 197–248.
[10] S. Singh, A.L. Pappachan, H.S. Gadiyar, Journal of the Less Common Metals, 120 (1986) 307–315.
[11] W.W. Wendlandt, J. Inorg. Nucl. Chem. 5 (1957) 118–122.
[12] W.W. Wendlandt, J. Inorg. Nucl. Chem. 9 (1959) 136–139.
[13] J.E. Powell, H.R. Burkholder, J. Inorg. Nucl. Chem. 14 (1960) 65–70.
[14] S.J. Ashcroft, C.T. Mortimer, J. Less-Common Met. 14 (1968) 403–406.
[15] V. Van Hong, J. Sundström, Thermochim. Acta 307 (1997) 37–43.
[16] G. Ren, X. Chen, Y. Pei, H. Li, H. Xu, J. Alloys Comp. 467 (2009) 120–123.
[17] G. Ren, Y. Pei, X. Chen, D. Yao, L. Qin, Z. Li, Nucl. Instrum. Methods Phys. Res., Sect. A 579 (2007) 11–14.
[18] O.G. Polyachenok, A.A. Iorbalidi, E.N. Dudkina, L.D. Polyachenok, Thermal stability and thermodynamics of LaCl$_3$ lowest hydrate, XVIII International Conference on Chemical Thermodynamics in Russia Samara, Russian Fedaration, October 3–7 2011.
[19] R.C. Weast, CRC Handbook of Chemistry and Physics, 69th ed., CRC Press, Florida, 1988–1989.
[20] F.H. Spedding, J.A. Rard, A. Habenschuss, J. Phys. Chem. 81 (11) (1977) 1069–1074.
[21] E.H.P. Cordfunke, R.J.M. Konings, Thermochim. Acta 375 (2001) 51–64.
[22] E.H.P. Cordfunke, R.J.M. Konings, Thermochim. Acta 375 (2001) 17–50.
[23] James.A. Sommers, Edgar.F. Westrum, J. Chem. Thermodyn. 8 (12) (1976) 1115–1136.
[24] R.J. Roy, G.J. Kipouros, Thermochim. Acta 178 (1991) 169–183.
[25] W. Judge, G.J. Kipouros, Can. Metall. Q. 52 (3) (2013) 303–310.
[26] J.M. Wang, Z.Z. Guo, Y.S. Chen, S.F. Huang, C.Y. Wang, Acta Chim. Sinica 48 (1990) 967–972.
[27] F.H. Spedding, C.W. DeKock, G.W. Pepple, A. Habenschuss, J. Chem. Eng. Data 22 (1) (1977) 58–70.
[28] S.R. Dharwadkar, A.S. Kerkar, M.S. Samant, Thermochim. Acta 217 (1993) 175–186.
[29] G.V. Belov, B.G. Trusor, ASTD-Computer aided reference book in thermodynamical, thermochemical and thermophysical properties of species, version 2, Moscow, 1983–1995.